Advances in Geo-Energy Research

Vol. 2, No. 3, p. 319-342, 2018
www.astp-agr.com

Original article

The workflow to analyze hydraulic fracture effect on hydraulic fractured horizontal well production in composite formation system

Jianwei Yuan[1], Ruizhong Jiang[1]*, Wei Zhang[2]

[1]*School of Petroleum Engineering, China University of Petroleum (East China), Qingdao 266580, P. R. China*

[2]*The Pennsylvania State University, University Park, PA 16802, United States*

(Received June 23, 2018; revised July 13, 2018; accepted July 14, 2018; available online July 21, 2018)

Citation:
Yuan, J., Jiang, R., Zhang, W. The workflow to analyze hydraulic fracture effect on hydraulic fractured horizontal well production in composite formation system. *Advances in Geo-Energy Research*, 2018, 2(3): 319-342, doi: 10.26804/ager.2018.03.09.

Corresponding author:
*E-mail: jrzhong@126.com

Keywords:
Tight oil reservoir
composite system
multistage fractured horizontal well
well testing

Abstract:
Hydraulic fracturing generally leads to highly complex hydraulic networks for tight oil reservoirs. It is significant to understand the hydraulic fracture effect on well performance. As an effective tool, semi-analytical solution for well pressure transient analysis (PTA) and rate transient analysis (RTA) is used in large amount because of higher calculation efficiency than numerical solution. In this paper, the PTA and RTA methods and result of composite formation system (CFS) are shown comprehensively. Firstly, a mathematical model of multistage fractured horizontal well (MsFHW) in CFS was proposed for tight oil reservoir with different regions and formation properties. In the model, two regions with different formation parameters were distinguished. This assumption of two regions, i.e. CFS is a composite tight reservoir formed after hydraulic fracturing. Difference of finite hydraulic fracture conductivity, inclined angle of hydraulic fracture, different shapes of multi-wing fractures in perforating point are considered to make this model powerful to analyze production performance of different MsFHW types. The inner and outer regions were assumed as dual porosity mediumbut single porosity medium model can also be solved by simplification. Then, the solution of MsFHW performance analysis model is obtained by source function method and the source function superposition principle which are common used in PTA and RTA. PTA for well producing at a constant production rate and RTA for well producing at a constant wellbore pressure were obtained and discussed. Different flow regimes were divided for different fracture geometry situations. The effects of different MsFHW types on PTA and RTA were analyzed. The inflow performance for different hydraulic fractures were presented.

1. Introduction

The development of tight oil and gas has become a hot issue all around the world (Howarth et al., 2011; Hughes, 2013; Vidic et al., 2013). As an effective tool, MsFHW receives an increasing attention owing to its advantages of reduced flow resistance, increased drainage area, and improved production. This new technique made it possible to develop the tight gas and oil reservoirs economically and leads to the shale gas and tight oil revolution (Patzek et al., 2013; Wang et al., 2014; Mănescu and Nuño, 2015).

Lab experiments, microseismic observations and geomechanics theoretical analysis show that hydraulic fractures can be complex geometry (Weng et al., 2014; Wu, 2014; Guo et al., 2015). Commonly, the hydraulic fracture will be a symmetrical bi-wing shape. But under certain conditions, complex hydraulic networks may exist and highly affects MsFHW production performance. When developing tight oil reservoirs, a large fracture network is beneficial to maximize well performance which is defined as stimulated reservoir volume (SRV) (Mayerhofer et al., 2010; Wang et al., 2015). The SRV can create high conductivity flow channels which benefit the oil or gas production (Stalgorova et al., 2012a, 2012b; Clarkson and Christopher, 2013). SRV makes it possible to develop tight oil or shale gas commercially (Mayerhofer et al., 2006; Duliman, 2013). Horizontal in situ stress difference, rock brittleness and natural fracture system are key factors to affect the morphology of SRV (Britt and Schoeffler, 2009; King, 2010). The effective fracture network mechanisms have been widely investigated both experimentally and numerically which provide effective guide for unconventional field development (Akulich and Zvyagin, 2008; Rahman et al., 2009;

https://doi.org/10.26804/ager.2018.03.09.

Chuprakov et al., 2011; Fan and Zhang, 2014).

Many scholars have done research on the production performance of MsFHW. Analytical and semi-analytical methods had been used. Pressure transient behavior of horizontal wells coupled with multiple hydraulic fractures were analyzed in single or dual porosity media and bi-wing shaped fractures, multi-wing shaped fractures and secondary-fracture were also considered (Chen et al., 2004; Zerzar et al., 2004; Luo and Tang. 2015). To consider the SRV, the tri-linear flow model was proposed to study the MsFHW performance in unconventional reservoirs and the transient pressure curves were given and used to analyze field data (Ozkan et al., 2009; Ozkan et al., 2011). Brown et al. (2011) presented an analytical tri-linear flow model to simulate the pressure transient and production behavior of fractured horizontal wells in unconventional reservoirs. The study provide an insight about possible flow regimes and the conditions leading to these flow regimes. Using a tri-linear flow model, Apaydin et al. (2012) presented an analytical model with composite matrix blocks to describe the effect of matrix micro-fractures on the effective matrix permeability. Stalgorova and Mattar (2013) improved the tri-linear flow model where SRV is simplified into a stimulated region with limited width. Five regions were defined to simulate the stimulated reservoir volumes. Flow in these regions was all linear. Sang et al. (2014) improved the tri-linear model by considering desorption and adsorption for shale gas reservoirs. Tian et al. (2014) established a new model considering adsorption, desorption, and dual diffusion. All tri-linear models are based on the assumption that fluid flow obeys the linear flow in discovered regions. This assumption may ignore some flow regimes compared with the actual production process in MsFHW reservoirs. There are other approaches to characterize the SRV. The key motivation is to overcome the constrains because of the linear region assumption. Xu et al. (2015) used the equivalent elliptical flow model to describe the SRV in which the reservoir was approximately a composite formation considering dual-porosity. The model divided the reservoir into inner and outer regions, and the inner region can be used to characterize the SRV, and the outer region is the non-stimulated reservoir volume. The mathieu modified functions were used to solve the elliptical flow problem successfully. Zhao et al. (2014) proposed a similar model using a circular region to characterize the SRV in tight gas reservoirs.

Numerical simulation has been a powerful and effective tool for studying SRV and fracture networks. Mayerhofer et al. (2006) performed numerical reservoir simulations to understand the impact of fracture-network properties including fracture size and density, fracture conductivity, matrix permeability and gaps in the network on well performance. Cipolla et al. (2010, 2011) presented a workflow for using micro seismic data to characterize discrete fractures. Meryer et al. (2011) presented a method to predict MsFHW performance with SRV using the discrete fracture network numerical simulation. Wang et al. (2015) studied flow regimes using the numerical simulation. Yu et al. (2015) studied the well spacing optimization and reservoir performance using numerical simulation in Bakken tight oil reservoirs. Weng et al. (2014) presented and validated a comprehensive and efficient complex fracture network model that simulates hydraulic fracture networks created during the stimulation treatment and proppant placement. Numerical reservoir simulation is an effective tool to obtain well performance, but usually with certain sacrifices on simulation accuracy and efficiency.

All above works are valuable to understand the MsFHW performance. To our best knowledge, there are few models which can successfully analyze the MsFHW performance including pressure transient analysis (PTA) and rate transient analysis (RTA) in a composite system of tight oil reservoirs. The models proposed previously can study the production performance of tight oil and gas in some extent (Jiang et al., 2014; Zhao et al., 2014) but have some limits: a) the hydraulic fracture conductivity is assumed to be infinite which can cause error in production performance. In fact, the hydraulic fracture has the finite conductivity; b) these models can't be used in the PTA and RTA when considering differences of geometry between different hydraulic fractures. In this paper, the MsFHW model in CFS is considered to be as dual-porosity media. In the matrix, the unsteady flow was considered which is very important for tight oil/gas reservoirs because it is not suitable to consider the pseudo-steady flow between the fracture and matrix (Ozkan et al., 2009). Also, the conductivity of hydraulic fracture is thoroughly considered. Different fracture geometries effects such as inclined fractures, geometry difference between different fractures are shown in detail.

The rest of this paper is organized as following. Section 2 describes the proposed model in detail; Section 3 presents the semi-analytical solution for the model. Detailed derivation is presented in Appendix B and Appendix C; Section 4 consists of results and discussion, where the type curves from the solutions and the impact of parameters are presented.

2. Model construction

In this section, we discuss the physical and mathematical models for understanding MsFHW performance in CFS.

2.1 Physical model

Due to the complexity of hydraulic networks, the SRV can be different shapes. Here, the circle shaped SRV (Jiang et al., 2014; Zhao et al., 2014) is focused. The schematic diagram for MsFHW in CFS is shown in Fig. 1. In the model, the reservoir is divided into inner and outer regions and the two regions have different reservoir properties. The inner region is a dual porosity media including matrix, natural fractures and induced fractures. The outer region is a dual porosity media which is not influenced by hydraulic fractures, but has natural fractures. Referring to our the model assumes: (1) tight oil pressure propagates slowly in the reservoir and is difficult to reach the boundary, so the outer region of a circular reservoir can be considered as infinite and the inner region radius is r_1; (2) the reservoir is horizontal with uniform thickness of h and original pressure p_i; (3) for the inner region, the horizontal permeability is noted as k_{f1}, the compressibility C_{tf1}, the

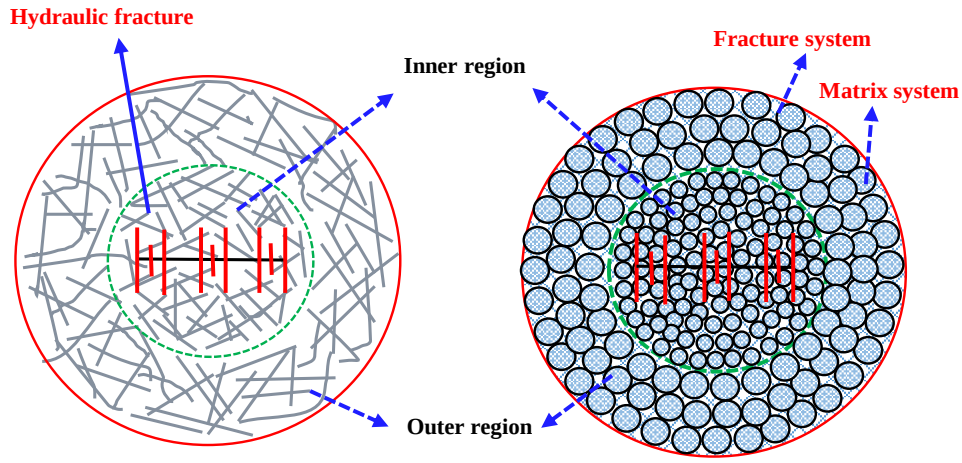

(a) Geology schematic of muti-stage horizontal well development

(b) Composite model in this paper

Fig. 1. Multi-stage horizontal well with circle shaped SRV.

porosity φ_{f1} for the fracture system; for the matrix, the permeability k_{m1}, the compressibility C_{tm1}, and the porosity φ_{m1}; while for the outer region, the same parameters as in the inner region are noted as k_{f2}, C_{tf2}, φ_{f2}, k_{m2}, C_{tm2}, φ_{m2} respectively; (4) MsFHW are completely included in the inner region (Fig. 1), and wells produce at a constant rate q_{sc}.

2.2 Mathematical model

2.2.1 Flow model in the inner region

For the matrix system, unsteady flow is considered. The flow equation in the inner region can be expressed as follows in the spherical coordinates system:

$$\frac{1}{r_{m1}^2}\frac{\partial}{\partial r_{m1}}\left(r_{m1}^2\frac{\partial p_{m1}}{\partial r_{m1}}\right)=\frac{\phi_{m1}\mu C_{tm1}}{k_{m1}}\frac{\partial p_{m1}}{\partial t} \quad (0\le r_{m1}\le R_1) \tag{1}$$

Initial condition:

$$p_{m1}\left(r_{m1},0\right)=p_i \tag{2}$$

Inner boundary condition:

$$\left.\frac{\partial p_{m1}}{\partial r_{m1}}\right|_{r_{m1}=0}=0 \tag{3}$$

Outer boundary condition:

$$\left.p_{m1}\right|_{r_{m1}=R_1}=p_{f1} \tag{4}$$

For the fracture system, the flow equation in the inner region is as follows with cylindrical coordinates system:

$$\frac{1}{r}\frac{\partial}{\partial r}\left(\frac{k_{f1}}{\mu}r\frac{\partial p_{f1}}{\partial r}\right)+q_{m1}=\phi_{f1}C_{tf1}\frac{\partial p_{f1}}{\partial t} \quad (0\le r\le r_1) \tag{5}$$

The outflow mass from unit volume of matrix per unit time is q_{m1}, according to the derivation of Jia et al. (2013). The inter-porosity gas mass flux from matrix system to fracture system per unit time from unit volume of matrix is:

$$q_{m1}=-\frac{3}{R_1}\frac{k_{m1}}{\mu}\left.\frac{\partial p_{m1}}{\partial r_{m1}}\right|_{r_{m1}=R_1} \tag{6}$$

With Eq. 1 - Eq. 6, the flow equation expressed in Laplace transform variables for the inner region can be expressed as Eq. 7. The derivation is presented in Appendix B.

$$\frac{1}{r_D}\frac{\partial}{\partial r}\left(r_D\frac{\partial\overline{p}_{f1D}}{\partial r_D}\right)=f_1\overline{p}_{f1D} \quad (0\le r_D\le r_{1D}) \tag{7}$$

Where:

$$f_1=\omega_1 u+3\lambda_1\left(\sqrt{\frac{1-\omega_1}{\lambda_1}u}\coth\left(\sqrt{\frac{1-\omega_1}{\lambda_1}u}\right)-1\right) \tag{8}$$

2.2.2 Flow model in the outer region

For the matrix system:

$$\frac{1}{r_{m2}^2}\frac{\partial}{\partial r_{m2}}\left(r_{m2}^2\frac{\partial p_{m2}}{\partial r_{m2}}\right)=\frac{\phi_{m2}\mu C_{tm2}}{k_{m2}}\frac{\partial p_{m2}}{\partial t} \quad (0\le r_{m2}\le R_2) \tag{9}$$

Initial condition:

$$p_{m2}\left(r_{m2},0\right)=p_i \tag{10}$$

Inner boundary condition:

$$\left.\frac{\partial p_{m2}}{\partial r_{m2}}\right|_{r_{m2}=0}=0 \tag{11}$$

Outer boundary condition:

$$p_{m2}\Big|_{r_{m2}=R_2} = p_{f2} \tag{12}$$

For the fracture system, the flow equation in the outer region is specified in the cylindrical coordinates system:

$$\begin{aligned}&\frac{1}{r}\frac{\partial}{\partial r}\left(\frac{k_{f2}}{\mu}r\frac{\partial p_{f1}}{\partial r}\right) - \frac{3}{R_2}\frac{k_{m2}}{\mu}\frac{\partial p_{m2}}{\partial r_{m2}}\Big|_{r_{m2}=R_2} \\ &= \phi_{f2}C_{tf2}\frac{\partial p_{f2}}{\partial t} \\ &(r_1 \le r \le \infty)\end{aligned} \tag{13}$$

With Eq. 9 - Eq. 13, the flow equation expressed in Laplace transform variables for the inner region can be expressed as Eq. 14. The derivation is presented in Appendix B.

$$\begin{aligned}&\frac{1}{r_D}\frac{\partial}{\partial r}\left(r_D\frac{\partial \overline{p}_{f2D}}{\partial r_D}\right) = f_2\overline{p}_{f2D} \\ &(r_{1D} \le r_D \le \infty)\end{aligned} \tag{14}$$

Where:

$$\begin{aligned}&f_2 = \omega_2 u\eta + 3\lambda_2\left(\sqrt{\frac{1-\omega_2}{\lambda_2}u\eta}\coth\left(\sqrt{\frac{1-\omega_2}{\lambda_2}u\eta}\right) - 1\right) \\ &(r_{1D} \le r_D \le \infty)\end{aligned} \tag{15}$$

2.2.3 Boundary condition and initial condition

For the line source inner region, the following equation can be derived for the inner region:

$$\lim_{r\to 0}\frac{2\pi k_{f1}hr}{\mu}\frac{\partial p_1}{\partial r} = -\tilde{q} \tag{16}$$

Assuming the upper and lower boundaries of formation are closed for the formation and the boundary of formation in horizontal direction is infinite, we can obtain the following equations:

$$\frac{\partial p_{f1}}{\partial z_1} = \frac{\partial p_{f2}}{\partial z_2} = 0,\ z = 0\ or\ h \tag{17}$$

$$p_{f2} = 0,\ r = \infty \tag{18}$$

For the inner region and outer region, when $r = r_1$, the pressure and flux will be continuous. So the interface condition will be:

$$p_{f1} = p_{f2},\ r = r_1 \tag{19}$$

$$\frac{\partial \overline{p}_{fD1}}{\partial r_D} = \frac{1}{M}\frac{\partial \overline{p}_{fD2}}{\partial r_D},\ r_D = r_{1D} \tag{20}$$

Applying the dimensionless variables and Laplace transformations to above Eq. 16 - Eq. 20, the following equations can be derived:

$$\lim_{r_D\to 0} r_D\frac{\partial \overline{p}_{f1D}}{\partial r_D} = -\frac{\overline{\tilde{q}}}{q_{sc}}\ line\ source\ in\ inner\ region \tag{21}$$

$$\frac{\partial \overline{p}_{f1D}}{\partial z_{1D}} = \frac{\partial \overline{p}_{f2D}}{\partial z_{2D}} = 0,\ z_D = 0\ or\ h_D \tag{22}$$

$$\overline{p}_{f2D} = 0,\ r_D = \infty \tag{23}$$

$$\overline{p}_{f1D} = \overline{p}_{f2D},\ r_D = r_{1D} \tag{24}$$

$$\frac{\partial \overline{p}_{f1D}}{\partial r_D} = \frac{1}{M}\frac{\partial \overline{p}_{f2D}}{\partial r_D} = 0,\ r_D = r_{1D} \tag{25}$$

M is the mobility ratio of the inner region and the outer region. Note the conventional mobility ratio is defined between two different fluids; but it is used to characterize the mobility ability difference of the inner region and the outer region. Eq. 7, Eq. 14 and Eq. 21 - Eq. 25 form the basic model for the composite reservoir with a point source. In next section, the solution of this model is derived.

3. Analytical solution

3.1 Solution methods

There are two methods to obtain pressure solutions for the model proposed in section 2.2. One is using point function method by Jiang et al. (2014) where the line source can be obtained by point function solution integral. The other one is to obtain line source solution directly by Zhao et al. (2014) according to characteristics of Dirac delta function and Bessel's function. Both methods can solve this model effectively but the method by Zhao et al. (2014) is relatively easy to derive. The pressure distribution for a line source is according to the work by Zhao et al. (2014):

$$\overline{p}_{N1} = \frac{\overline{\tilde{q}_L}\mu}{2\pi k_{f1}h}\left[K_0\left(\sqrt{f_1}R_D\right) + \frac{M\sqrt{f_1}K_1\left(\sqrt{f_1}r_{1D}\right)K_0\left(\sqrt{f_2}r_{1D}\right) - \sqrt{f_2}K_0\left(\sqrt{f_1}r_{1D}\right)K_1\left(\sqrt{f_2}r_{1D}\right)}{M\sqrt{f_1}I_1\left(\sqrt{f_1}r_{1D}\right)K_0\left(\sqrt{f_2}r_{1D}\right) - \sqrt{f_2}I_0\left(\sqrt{f_1}r_{1D}\right)K_1\left(\sqrt{f_2}r_{1D}\right)}I_0\left(\sqrt{f_1}R_D\right)\right] \tag{26}$$

$$\overline{p}_{N2} = \frac{\overline{\tilde{q}_L}\mu}{2\pi k_{f1}h}\left[\frac{M\sqrt{f_1}K_0\left(\sqrt{f_1}r_{1D}\right)I_1\left(\sqrt{f_1}r_{1D}\right) + M\sqrt{f_1}K_1\left(\sqrt{f_1}r_{1D}\right)I_0\left(\sqrt{f_1}r_{1D}\right)}{M\sqrt{f_1}K_0\left(\sqrt{f_2}r_{1D}\right)I_1\left(\sqrt{f_1}r_{1D}\right) + \sqrt{f_2}I_0\left(\sqrt{f_1}r_{1D}\right)K_1\left(\sqrt{f_2}r_{1D}\right)}K_0\left(\sqrt{f_2}R_D\right)\right] \tag{27}$$

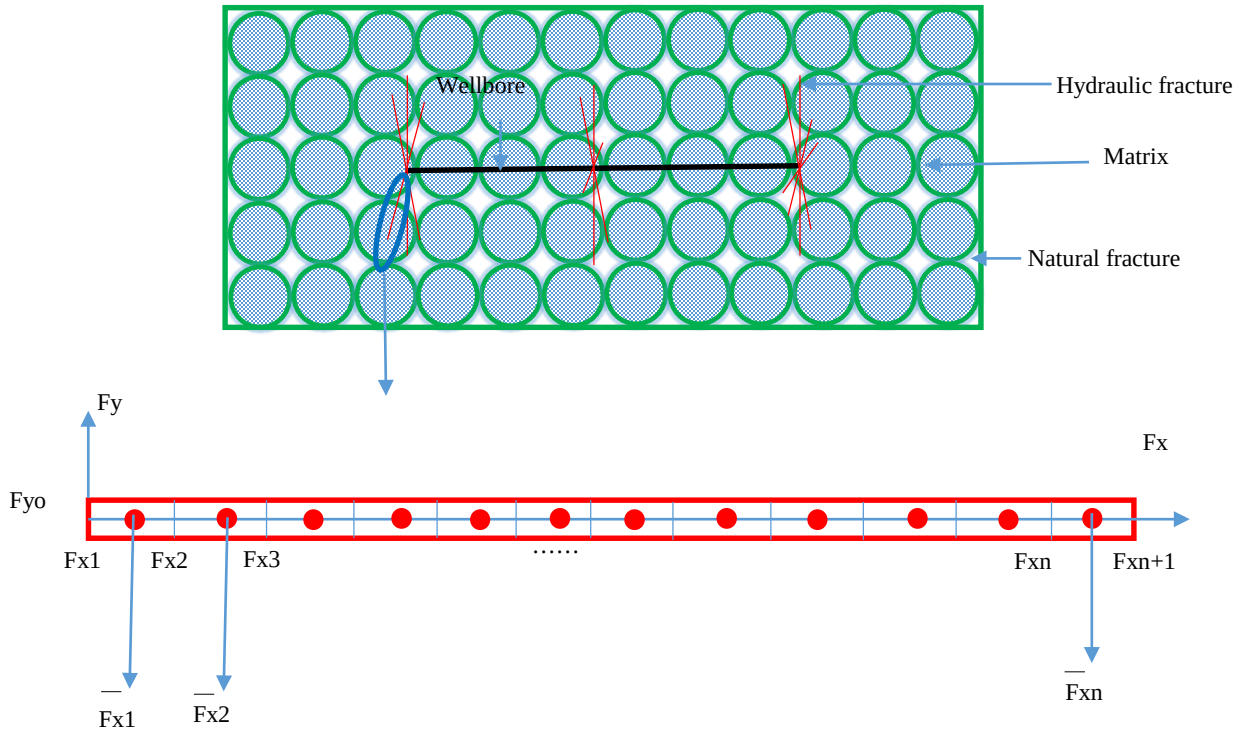

Fig. 2. A schematic illustration of multistage fractured horizontal well and fracture discrete units.

Where $\tilde{q}_L$ is the line source, m^3/s; R_D is the distance between the line source and pressure observation point; P_{N1} is line source solution when pressure observation point is in the inner region; P_{N2} is line source solution when pressure observation point is in the outer region.

3.2 Pressure behaviors for MsFHW in tight oil reservoirs considering SRV

The proposed model is simplified to obtain the pressures and rate behaviors for MsFHW. The following assumptions are made.

1) the wellbore to be intersected by N single-wing fractures, and all the fractures are transverse to the well and fully-penetrating to the formation shown in Fig. 2;

2) the flow from the reservoir to the wellbore is negligible comparing to the flow from the hydraulic fracture planes;

3) the well is assumed to produce at a constant rate or constant wellbore pressure.

To consider the finite conductivity fracture in transient pressure or rate analysis, the method proposed by Zerzar and Bettam (2004) and Luo et al. (2015) was used. The detailed derivation is presented in Appendix C. Eq. C-16 couples the wellbore pressure and the inflow flux for each fracture discrete units. Then, the superposition principle by Zhao et al. (2014) can be used to obtain the wellbore pressure and inflow flux for each fracture discrete units. Each single wing fracture has been discretized into n units, as shown in Fig. 2. There is $n*N+1$ equations which can solve $n*N+1$ unknowns of p_{wD}, q_{D1}, q_{D2}, … , q_{Dn*N}. Therefore, the bottomhole pressure distribution as well as flux distribution for each fracture can be obtained. The Gauss elimination method was first used to solve equations, then the Stehfest numerical inversion algorithm (Stehfest, 1970) was chosen to calculate the dimensionless bottomhole pressure as well as the dimensionless production rate distribution in real time space. The dimensionless well production rate at a constant bottomhole pressure can be defined as follows (Van et al., 1949):

$$\overline{q}_D = \frac{1}{u^2 \overline{p}_{wD}} \tag{28}$$

4. Results and discussion

In this section, the dimensionless pressure/rate and derivative response for a multistage fractured horizontal well in tight oil reservoirs are obtained with the model proposed above. The effects of different types of fractured wells on the behavior are studied.

4.1 Verification

In this model, if some parameters are set to satisfy some conditions, this new model proposed in this paper can be converted into some other models. If we set $\eta = 1$, $\omega_1 = 1$, and $\omega_2 = 1$, i.e., $f_1 = f_2 = u$, this new model can be simplified as single-porosity model in a homogenous reservoir, which is similar to the model proposed by Luo et al. (2014) and Zerzar et al. (2004). As shown in Fig. 3, very good match

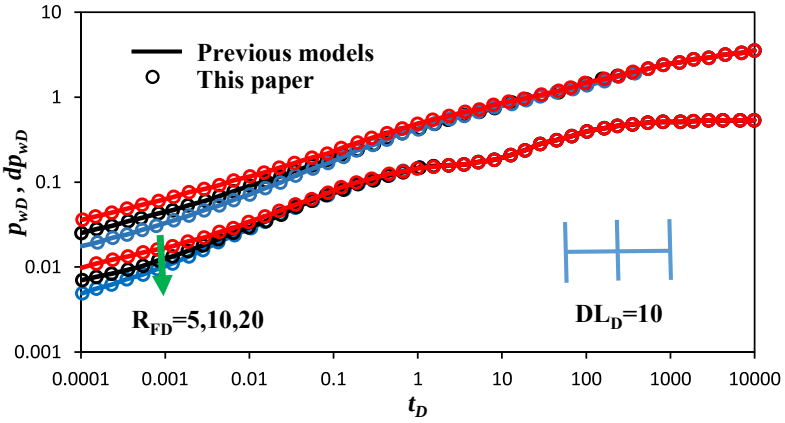

Fig. 3. Comparison of pressure and pressure derivative for multistage fractured horizontal well by 6 single-wing shaped hydraulic fractures.

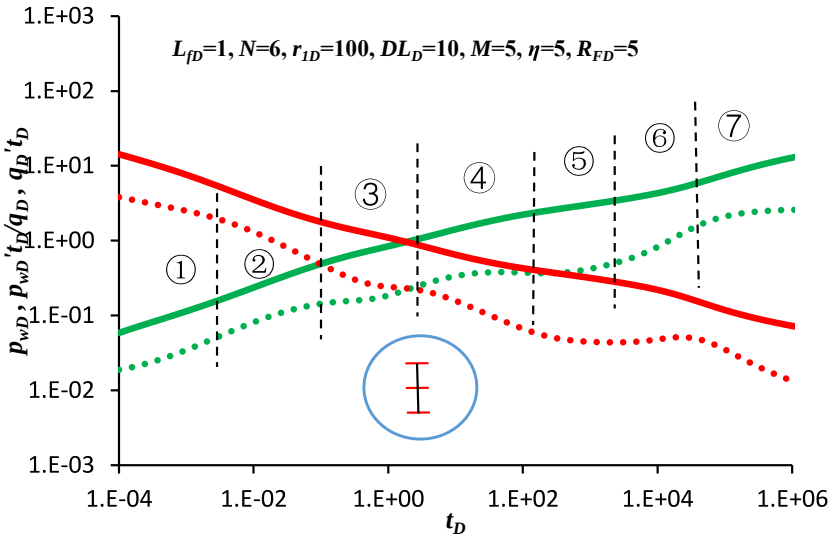

(a) Pressure and rate transient curves: the green lines shows the bottomhole pressure curve (the above one) and pressure derivative curve (the below dotted one); the red lines shows the well rate curve (the above one) and rate derivative curve (the below dotted one)

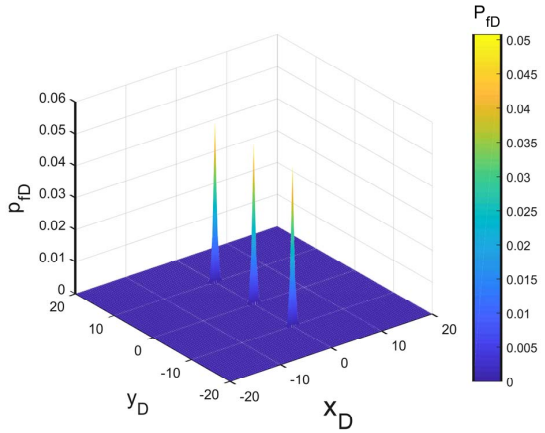

(1) Bilinear flow at t_D=8.11×10^{-4}

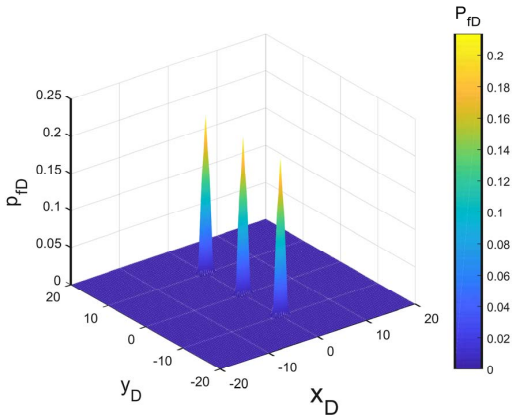

(2) Linear flow at t_D=8.11×10^{-2}

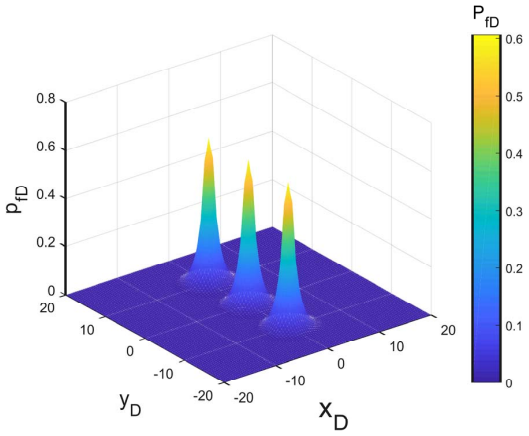

(3) First radial flow at t_D=2.31

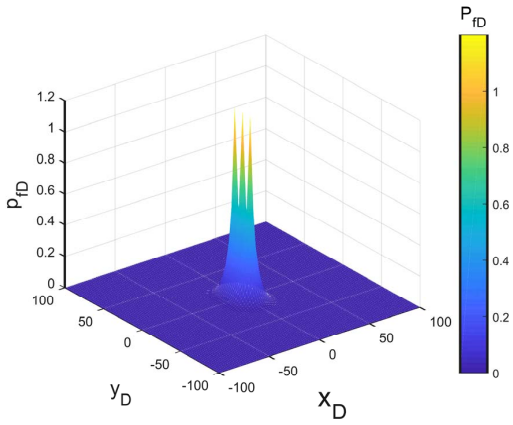

(4) Second linear flow at t_D=43.3

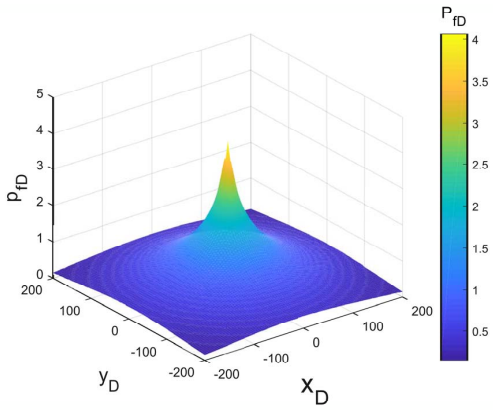

(5) First radial flow at t_D =534

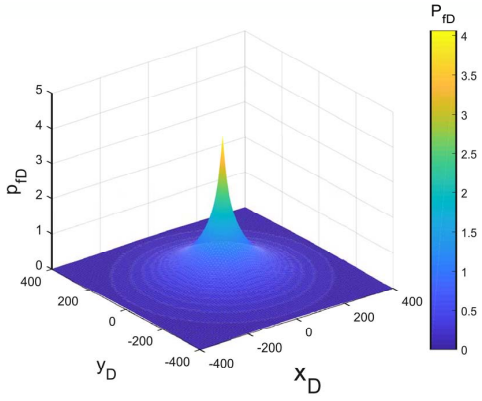

(6) transition flow at t_D =23100

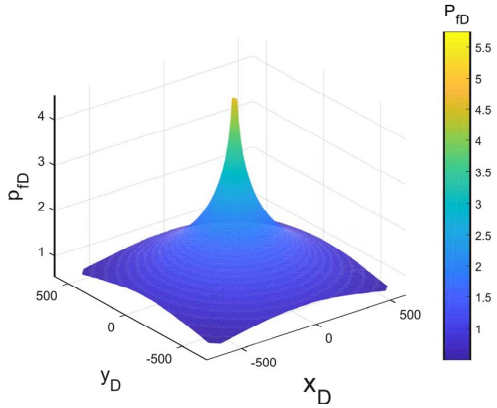

(7) transition flow at t_D =433000

(b) Dimensionless pressure at different time of each flow regime

Fig. 4. Flow regimes: multistage fractured well of single porosity media.

is obtained in the pressure and pressure derivative profiled compared results from our model and those from existing models. The comparison validated the proposed model.

4.2 Type curves of different multistage fractured wells

In this section, the dimensionless pressure/rate and derivative response for a multistage fractured horizontal well in tight oil reservoirs are obtained with the model proposed above.

Fig. 4 shows the type curves of MsFHW in single porosity media composite system by setting ω_1 = 1, and ω_2 = 1, i.e., $f_1 = u$ and $f_2 = \eta u$. The flow regimes are as follows: (1) the early bilinear flow period characterized by a slope of 1/4 in the pressure derivative curve; (2) the early linear flow characterized by a slope of 1/2 in the pressure derivative curve. During the first linear flow, each fracture produces independently with the oil flowing perpendicular to the fracture; (3) the early radial period around individual fractures marked by a constant pressure derivative which is 1/(4*N) on the type curve. This regime can occur if the fracture spacing is large enough compared to the fracture half-length; (4) the second linear flow period by a slope of 1/2 in the pressure derivative curve; (5) the second radial flow by a horizontal straight line in the derivative curve which is 1/2; (6) the transition flow period between second radial flow and the third radial flow; (7) the third radial flow characterized by a 1/2*M horizontal straight line in the derivative curve. Compared with the type curves for horizontal wells in the homogenous single porosity reservoir (shown in Fig. 3, there are three more flow regimes for the MsFHW in composite system, as shown as regimes (6) and (7) in Fig. 4a. Fig. 4b shows the 3D maps for the seven flow regimes discussed above. As can be seen, as time increases, pressure will spread from near the hydraulic fracture to away from it. In regime four, hydraulic fractures begin to interfere with each other. In regime six, pressure spreads to the outer region and the pressure and rate transient curves reflects the outer region formation parameters.

Fig. 5 shows the typical curve of multistage fractured well of dual porosity media. Fig. 5a shows two kinds of fractured well types. The first is that the hydraulic fractures are symmetrical along the wellbore which is the most popular fracture distribution type in hydraulic fracturing. The second is single wing along the wellbore. Fig. 5b shows the dimensionless pressure distribution of different flow regimes. Compared with the typical curve of MsFHW in single media composite system, for dual porosity media, regime five is much different from the single porosity media model. The "downward tip" in pressure derivative curve appears which reflects the inter-porosity flow between the matrix and natural fracture. Also, the second radial flow is recovered by the "downward tip". For symmetrical and single wing fractures models, the pressure spreads symmetrically for symmetrical fractures model at the early time while for single wing fractures model the pressure spreads fast on the side the factures distributes. Also, at the early time, the single wing fracture model consumes more energy which makes the pressure drop bigger. The reason is that the drainage area for single wing fracture is much less than the symmetrical one.

Though our purpose in this paper is to use the methods of the PTA and RTA for MsFHW, the model can also analyze the PTA and RTA for vertical fractured well in CFS. Fig. 6 shows the typical curve of vertical inclined fractured well with multiple-wings. The inclined angles are 0°, 60°, 120°, 180°, 240°, and 300° respectively. As can be seen from Fig. 6, five flow regimes can be divided: the early bilinear flow; the transition flow period between early bilinear flow and the first radial flow; inter-porosity flow between the matrix and natural fracture; the transition flow period between inter-porosity flow between the matrix and natural fracture and the third radial flow; the second radial flow. Compared to Fig. 4, the first radial flow regime and second regime both disappear for vertical inclined fractured well. The linear flow is not obvious for this model because the early time pressure interferes between different single wings.

Fig. 7 shows the typical curve of multi-stage and multi-

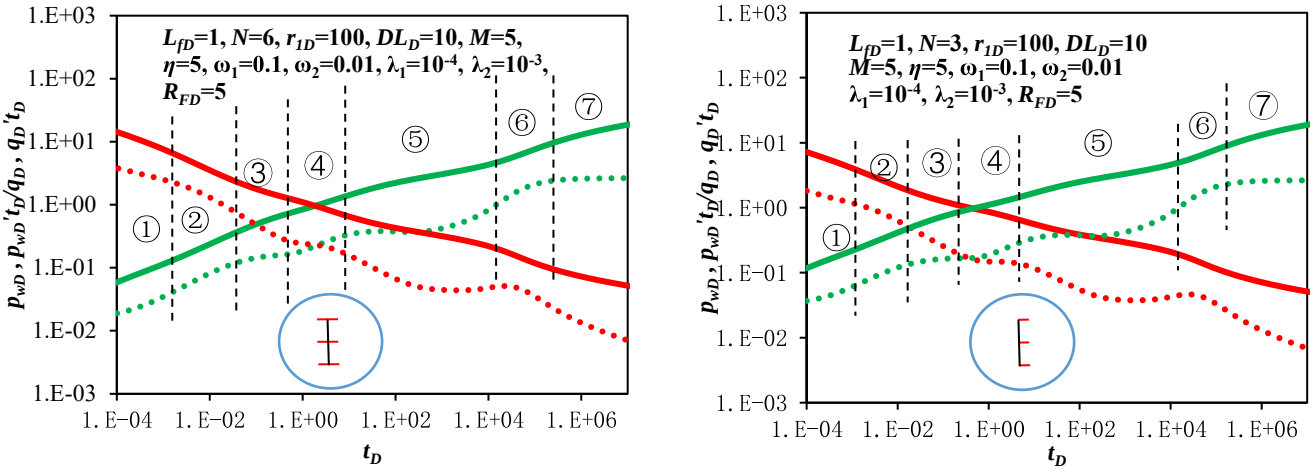

(1) symmetrical fractures

(2) single wing fractures

(a) Pressure and rate transient curves

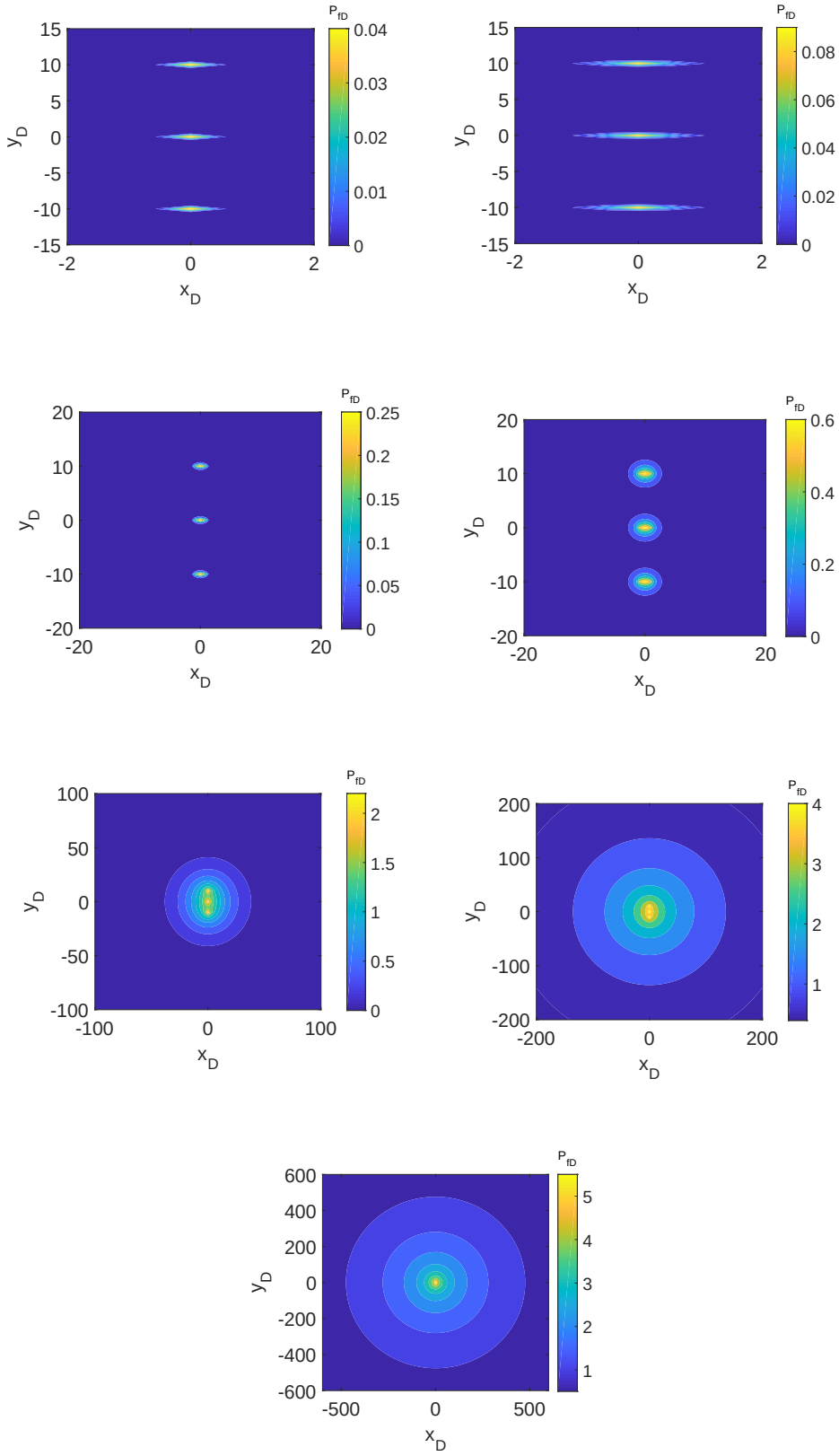

(1) Dimensionless pressure at different time of each flow regime(symmetrical fractures)

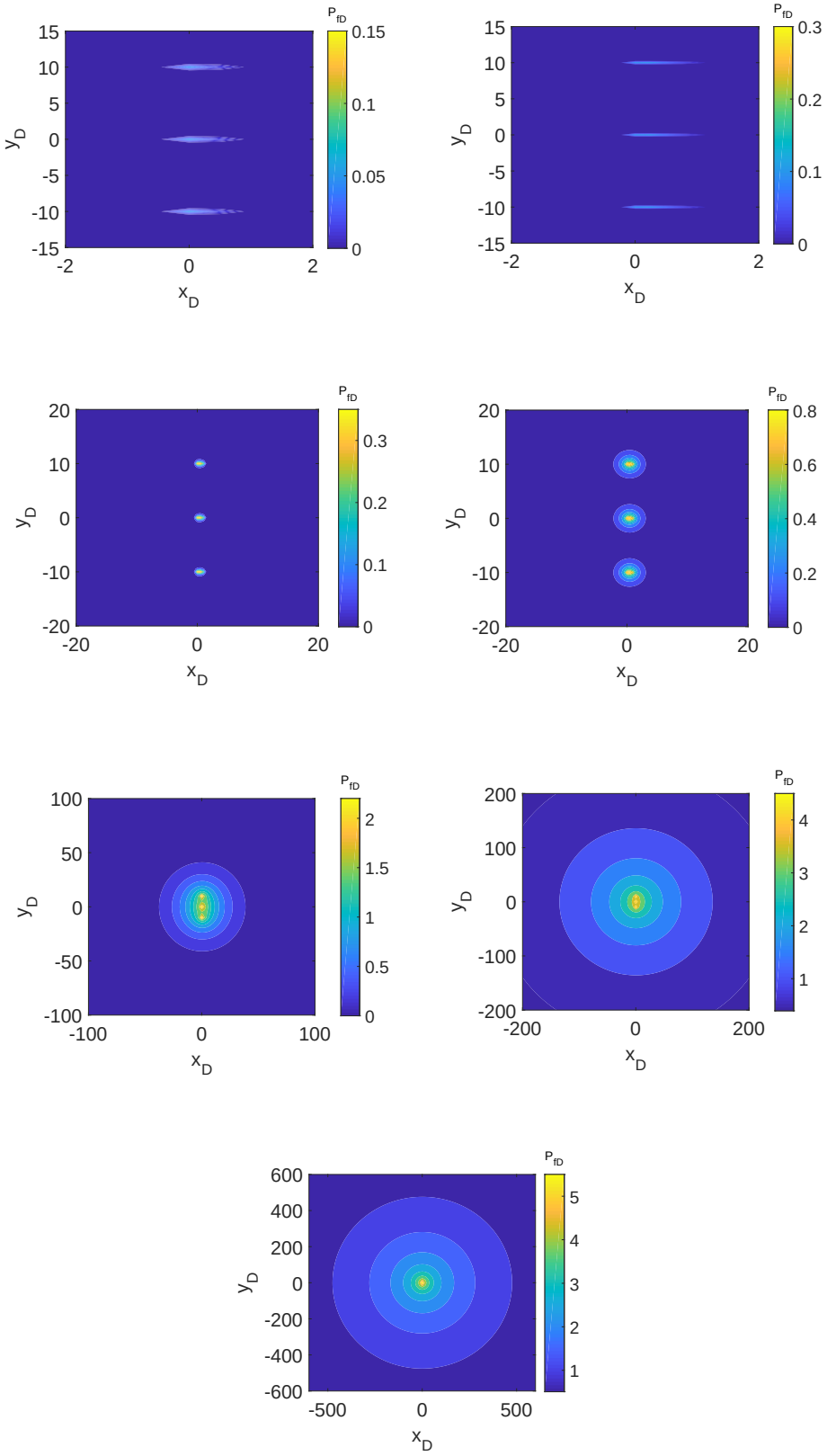

(2) Dimensionless pressure at different time of each flow regime(single wing fractures)

(b) Dimensionless pressure distribution of different flow regimes at different dimensionless times: t_D =0.000534, 0.00658, 0.187, 3.51, 534, 53400, 658000 respectively

Fig. 5. Flow regimes: multistage fractured well of dual porosity media with symmetry fractures and multistage fractured well of dual porosity media with single wing fractures.

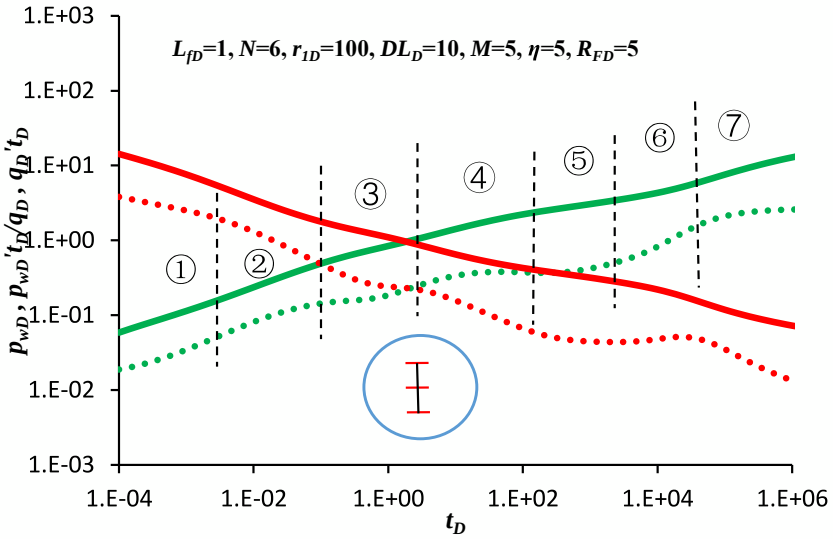

(a) Pressure and rate transient curves

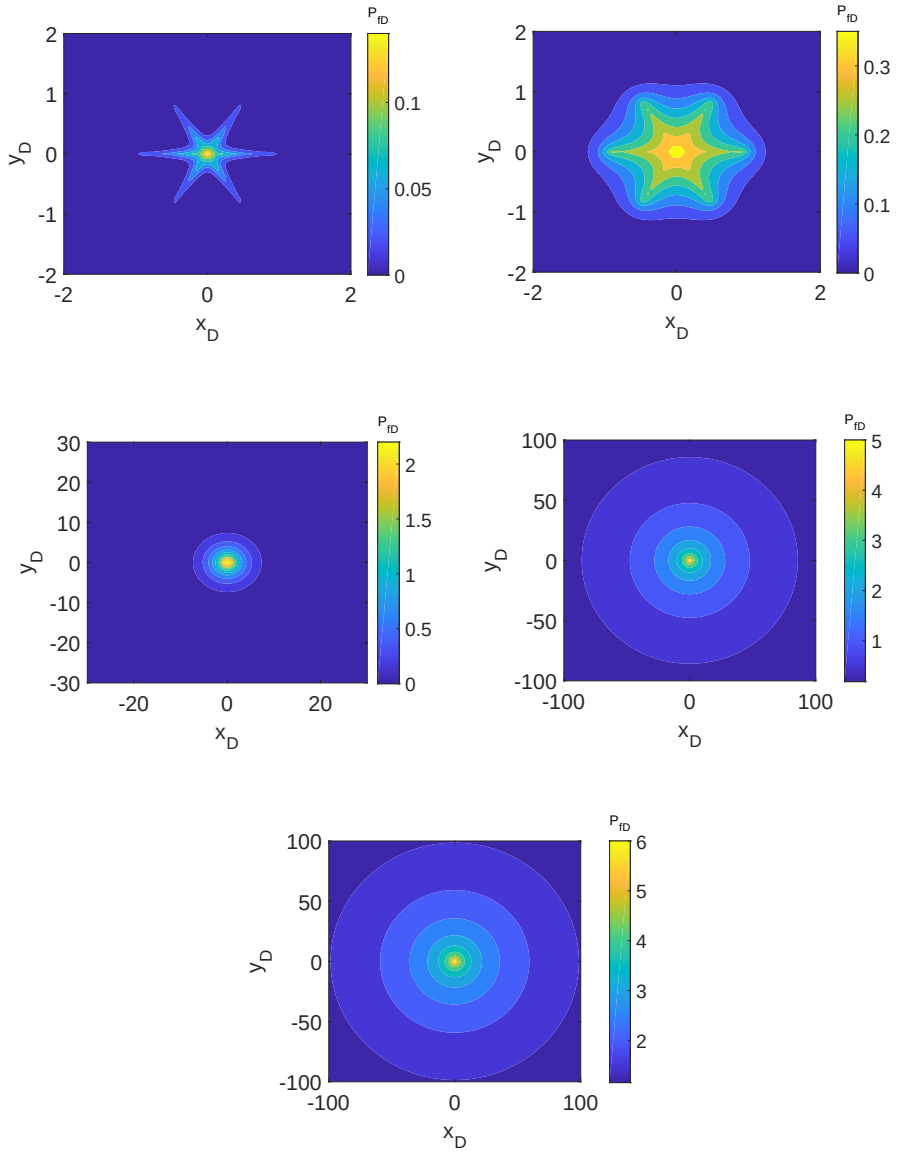

(b) Dimensionless pressure distribute of different flow regimes: t_D =0.000231, 0.00658, 18.7, 6580, 81100

Fig. 6. Flow regimes: multistage fractured vertical well of dual porosity media.

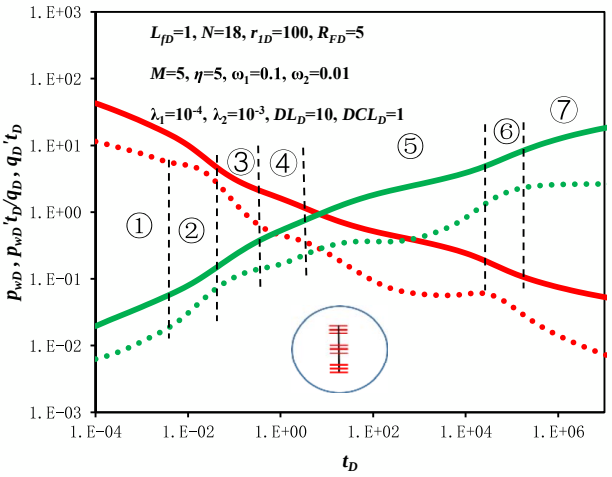

(1) multi-stage multi-cluster fractured well

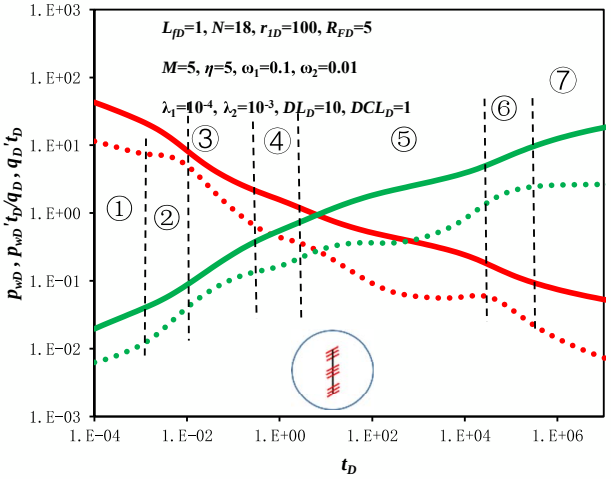

(2) multi-stage multi-cluster well with inclined fractured

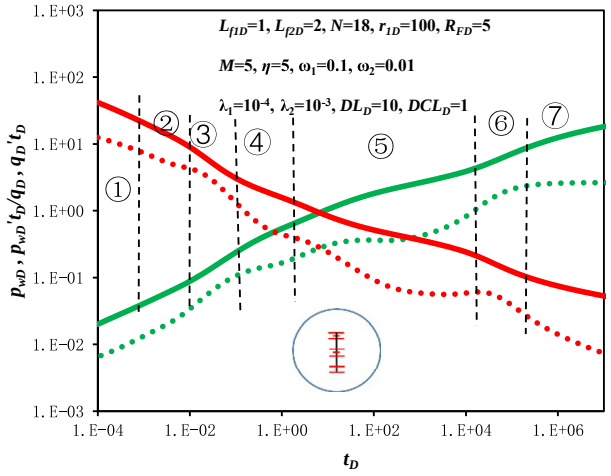

(3) multi-stage multi-cluster fractured well with unequal length fractures

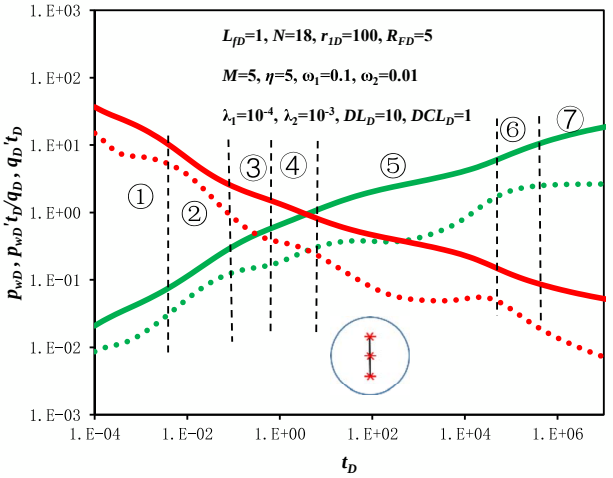

(4) multi-stage multi-cluster well with multi-wing fractures

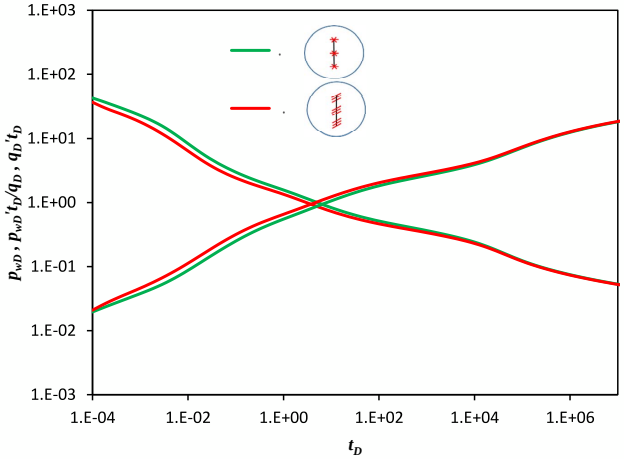

(5) Comparison of different fracture shapes

(a) Pressure and rate transient curves

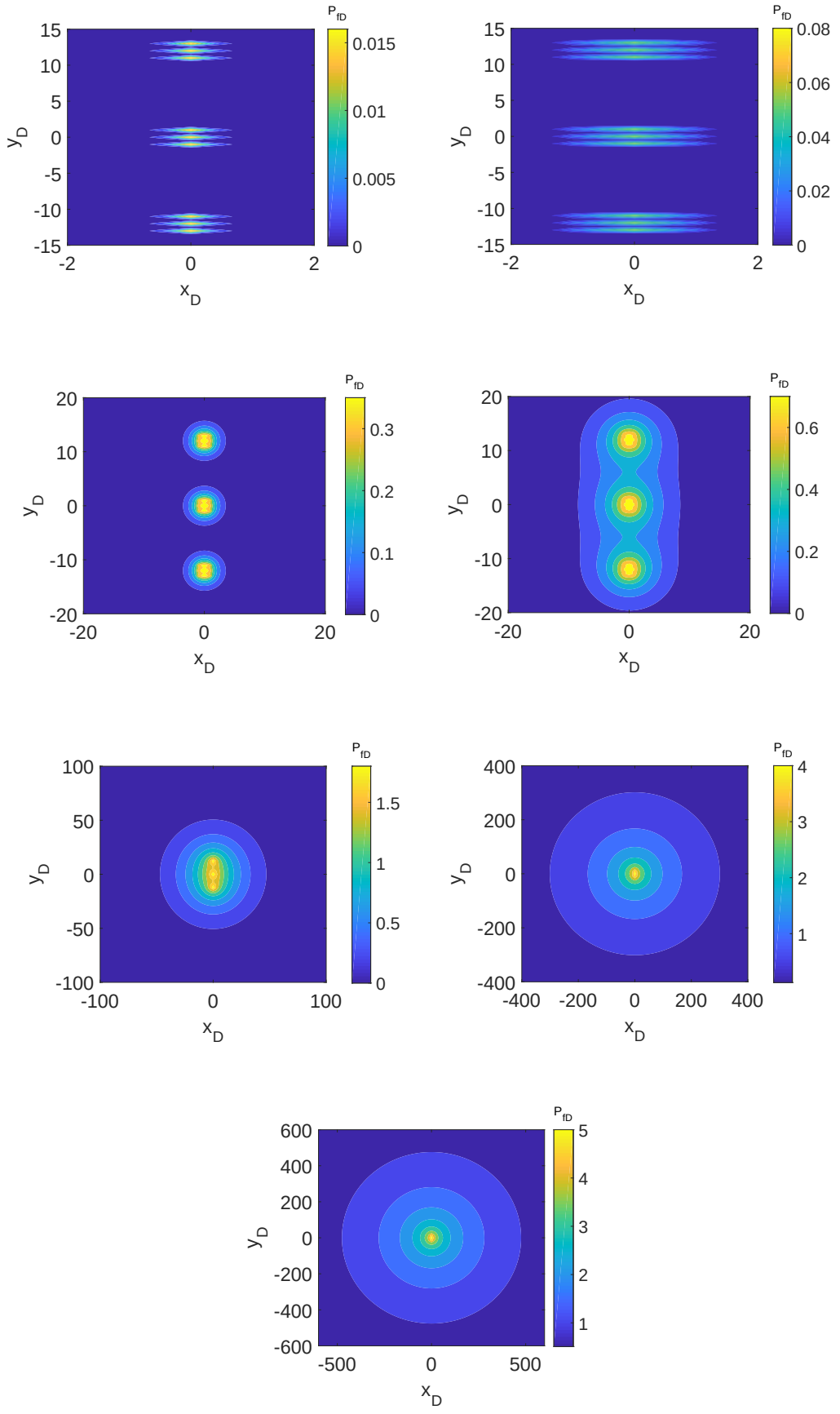

(1) multi-stage multi-cluster fractured well of dual porosity media

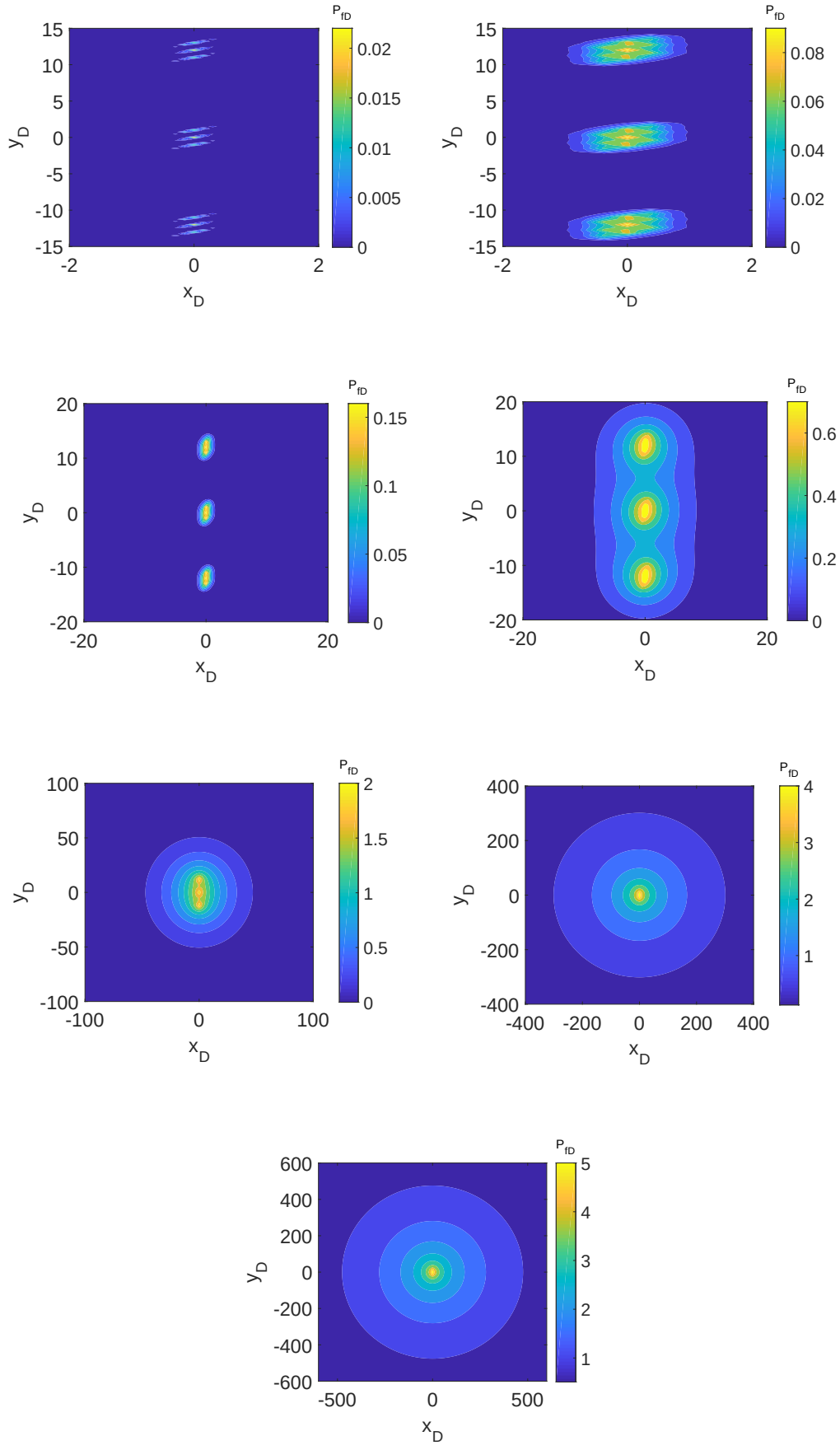

(2) multistage multi-cluster fractured well of dual porosity media with inclined fractures

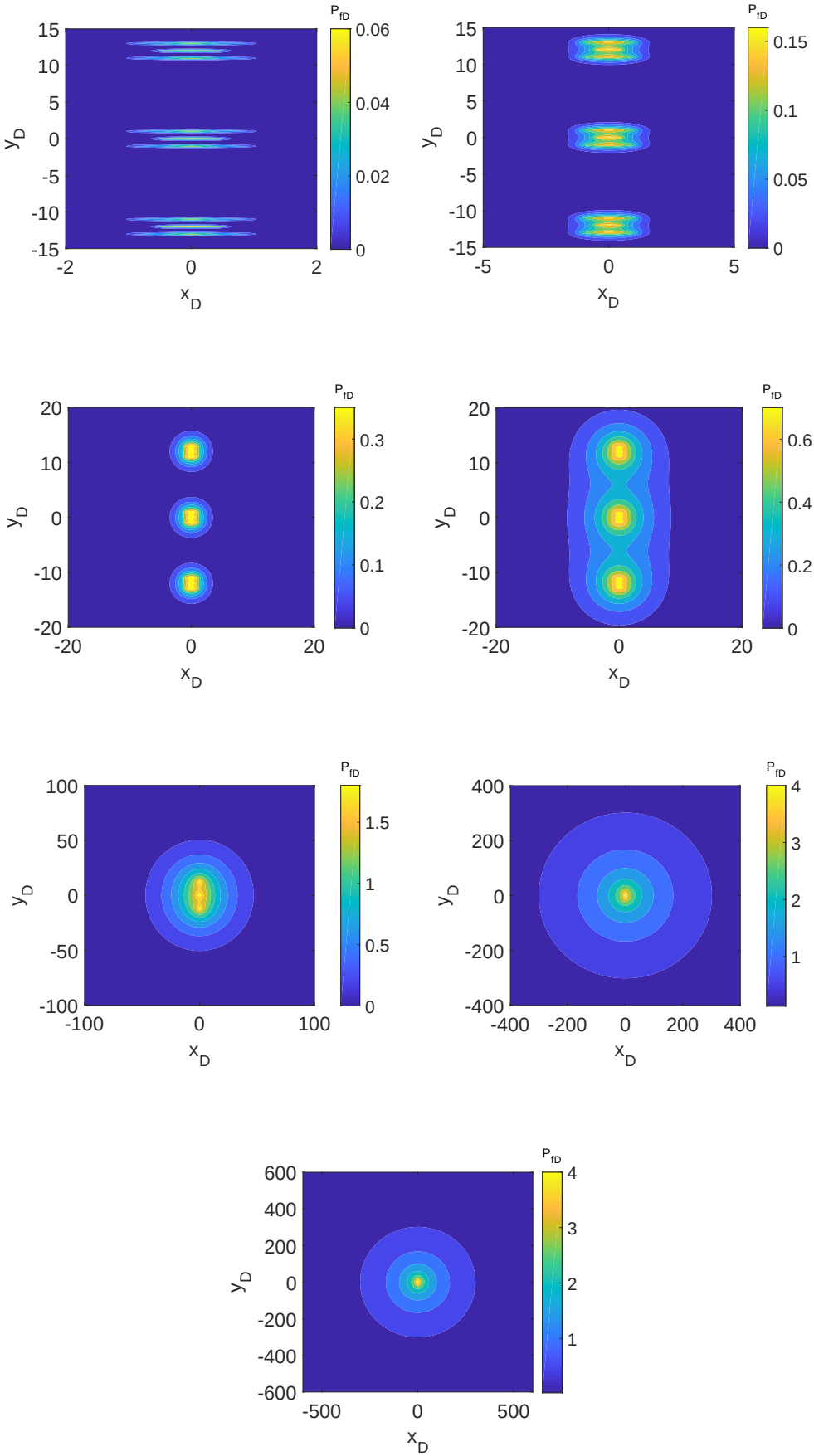

(3) multistage multi-cluster fractured well of dual porosity media with different length fractures

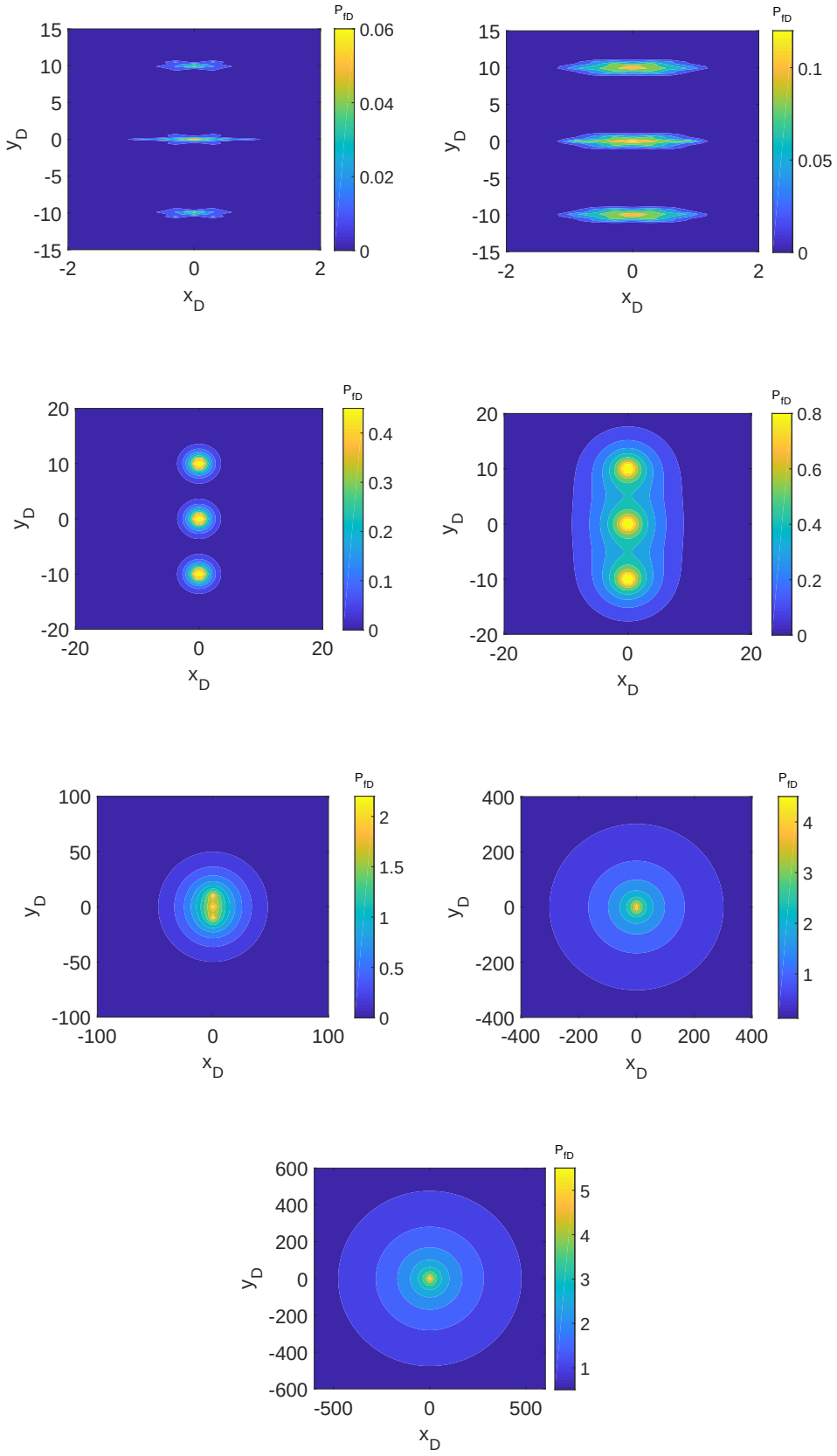

(4) multistage multi-cluster fractured well of dual porosity media with multiple wings fractures
(b) Dimensionless pressure distribute of different flow regimes: t_D =0.000811, 0.035, 0.43, 3.5, 811, 81113, 657933

Fig. 7. Flow regimes: multi-stage multi-cluster fractured well of dual porosity media; multi-stage multi-cluster fractured well of dual porosity media with inclined fractures; multistage multi-cluster fractured well of dual porosity media with different length fractures; multistage multi-cluster fractured well of dual porosity media with multiple wings fractures.

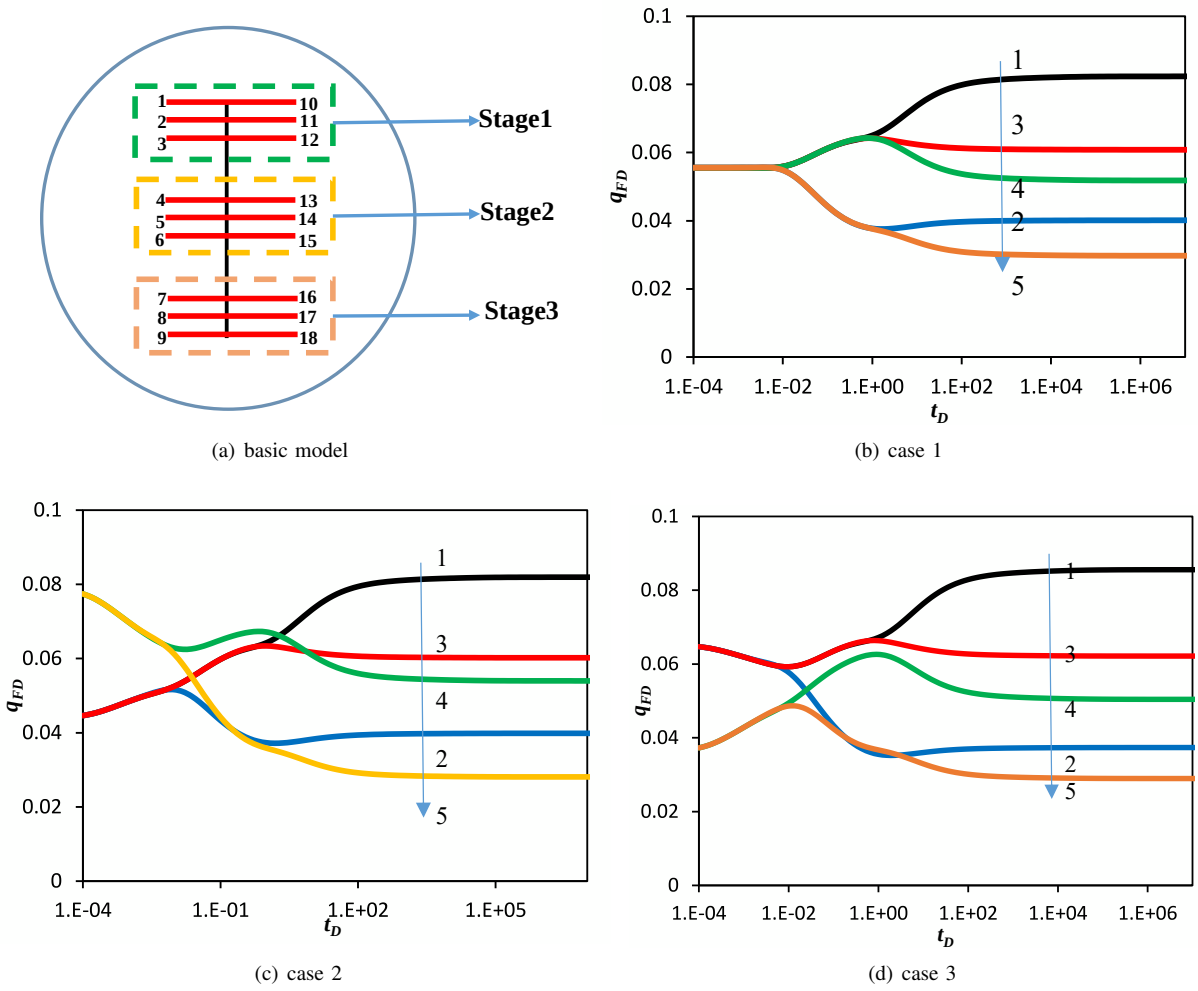

(a) basic model

(b) case 1

(c) case 2

(d) case 3

Fig. 8. Inflow performance of different stage fracture conductivity.

cluster fractured horizontal well, multi-stage and multi-cluster inclined fractured well (the inclined angle is 60°), multi-stage and multi-cluster inclined fractured well with different length fractures, and multi-stage and multi-cluster well with multi-wing fractures (inclined angle is 0°, 60°, 120°, 180°, 240°, and 300°). When developing tight oil/gas, multi-stage and multi-cluster fractured well always be used. For a multi-stage and multi-cluster fractured well, each stage contains a certain number of fractures which called "cluster" (Jia et al., 2013). In Fig. 7, there are three stages and for each stages there are six single wing fractures. The dimensionless distance between stages is DL_D = 10 and the dimensionless distance between cluster fractures is DCL_D = 1. Also seven flow regimes exist: the early bilinear flow period; the transition flow period between early bilinear flow and the first radial flow; the first radial flow; the linear flow period; inter-porosity flow between the matrix and natural fracture; the transition flow period between inter-porosity flow between the matrix and natural fracture and the third radial flow; the second radial flow. As can be seen, for these four model, the differences between each other focus on the first, second and third flow regimes. At the early time, pressure spreads near the wellbore and different hydraulic facture geometries have important effect on early flow regimes.

4.3 Fracture inflow performance

It is important to understand contribution of each fractures to the total wellbore. In section 4.2, PTA and RTA of different well types are presented. In this part, we will show how to use the proposed model to analyze the inflow performance of different fractures. After inflow flux distribution of each fracture were got by using the method proposed in section 3.2, it is easy to obtain the fracture inflow performance of multistage fractured horizontal well in composite system by sum the flux of each discrete unit related to the facture, i.e., $\sum_{i=1}^{n} q_{Dn}$. We take the multi-stage multi-cluster fractured well shown in Fig. 7a(1) as example. Also, as comparisons, different fracture conductivity are set for different stages:

Case 1: R_{FD}(stage 1) = R_{FD}(stage 2) = R_{FD}(stage 3) = 5;

Case 2: R_{FD}(stage 1) = R_{FD}(stage 3) = 5; R_{FD}(stage 2) = 15;

Case 3: R_{FD}(stage 1) = R_{FD}(stage 3) = 15; R_{FD}(stage 2) = 5.

Fig. 8 shows the inflow rate of different cases. As the geometry model is symmetry, only five fractures are studied. As can be been from Fig. 8b, Fig. 8c and Fig. 8d, these three cases are different for the inflow rates of different stage fracture stages. For case 1, at the early time, each fracture has the same inflow rate because the conductivities are same for different factures. Then, 1, 3, and 4 have a big rate and keep same. 2 and 5 keep a small rate. During this period, 1, 3 and 4 have the same drainage area and bigger than 2 and 5 which have smaller drainage area. At the later time, fracture 1 has the biggest inflow rate because the drainage area is the biggest for among these fractures. On the contrary, fracture 5 has the smallest inflow rate because it has the smallest drainage area at the center position. For case 2, at the beginning, fracture 4 and 5 have the biggest inflow rate because the high fracture conductivity. Also, for case 3, in early time, fracture 1, 2, and 3 have the biggest inflow rate because the high fracture conductivity. As time goes on, the inflow characteristics are like the case 1 and the hydraulic fracture has weak effect on inflow performance and the drainage area becomes the key factor.

5. Conclusions

In this paper, a new model is proposed for a multistage fractured horizontal well in composite tight oil reservoirs. The pressure transient and rate transient responses are discussed. The following conclusions can be drawn from this study:

(1) Oil flow in tight reservoirs is complicated because of complex fracture and matrix systems for MsFHW. In the paper, the mathematical model is verified to describe the flow both in MsFHW and matrix. Specifically, the composite system is taken into consideration compared to the existing PTA and RTA method in tight oil reservoirs. Seven flow regimes are identified from the transient pressure curve for single porosity media and dual porosity media formations for symmetrical bi-wing fracture MsFHW. The pressure transient and rate transient curves are different for these two kinds of well models.

(2) The fracture geometry has a significant effect on pressure and rate transient curves. Flow regimes for multi-stage muti-cluster fractured well of dual porosity media, multi-stage muti-cluster fractured well of dual porosity media with inclined fractures, multi-stage muti-cluster fractured well of dual porosity media with different length fractures, and multi-stage muti-cluster fractured well of dual porosity media with multiple wings fractures are different in the early time and in the late time they keep constant in the pressure and rate transient curves.

(3) The workflow proposed in this paper can be used to analyze the inflow performance for MsFHW. The rate of each fracture can be calculated exactly at the production life of a certain well type. If the properties are same for different fractures. The early inflow performances are same because there is no interference between fractures. When production time increases, the inflow performance of different fractures becomes much different because the fracture position decides the different oil drainage area at late time. When the properties of fractures are different, the inflow performance are different at the early time because the near wellbore resistance are improved in different extent. But by comparing the four models in Fig. 7a(5), if the formation parameters are same, the later inflow performance are the same for different fractures under different properties.

Nomenclature

M = Mobility ratio, fraction
k = Permeability, m^2
μ = Fluid viscosity, Pa·s
η = Diffusivity ratio, fraction
u = Laplace space variable with respect to t_D
h = Reservoir thickness, m
L = Reference length, m
$I_k(x)$ = The modified Bessel function of first kind
$K_k(x)$ = The modified Bessel function of second kind
q_{sc} = Production rate, m^3/s
L_f = Fracture half length, m
t = Time, s
N = Facture number
DL = Stage spacing, m
DCL = Cluster fractures, m
r, θ, z = Directional coordinates
φ = Porosity, fraction
c_t = Total compressibility, Pa^{-1}
p = Pressure, Pa
ω = Storability coefficient
λ = Inter-porosity coefficient
q = Point source, m^3/s
Fx = Distance of discrete units in X direction
Fy = Distance of discrete units in Y direction
W = Hydraulic fracture width

Subscripts and superscripts

D = Dimensionless
i = Initial
m = Matrix
f = Fracture
$-$ = Laplace domain
1 = Inner region
2 = Outer region
F = Hydraulic fracture

Acknowledgments

This study was funded by National Science and Technology Major Project (No.2017ZX05013-002).

References

Akulich, A.V., Zvyagin, A.V. Interaction between hydraulic and natural fractures. Fluid Dynam+. 2008, 43(3): 428-435.

Apaydin, O.G., Ozkan, E., Raghavan, R. Effect of discontinuous microfractures on ultratight matrix permeability of a dual-porosity medium. SPE Reserv. Eval. Eng. 2012, 15(4): 473-485.

Biryukov, D., Kuchuk, F.J. Pressure transient behavior of horizontal wells intersecting multiple hydraulic fractures in naturally fractured reservoirs. Transport Porous Med. 2015, 110(3): 369-408.

Britt, L.K., Schoeffler, J. The geomechanics of a shale play: what makes a shale prospective. Paper SPE125525 Presented at the SPE Eastern Regional Meeting, Charleston, West Virginia, USA, 23-25 September, 2009.

Brown, M., Ozkan, E., Raghavan, R., et al. Practical solutions for pressure-transient responses of fractured horizontal wells in unconventional shale reservoirs. SPE Reserv. Eval. Eng. 2011, 14(6): 663-676.

Chen, Z., Liao, X., Zhao, X., et al. A semianalytical approach for obtaining type curves of multiple-fractured horizontal wells with secondary-fracture networks. SPE J. 2016, 21(2): 538-549.

Chuprakov, D.A., Akulich, A.V., Siebrits, E., et al. Hydraulic-fracture propagation in a naturally fractured reservoir. SPE Prod. Oper. 2011, 26(1): 88-97.

Cipolla, C.L., Fitzpatrick, T., Williams, M.J., et al. Seismic-to-simulation for unconventional reservoir development. Paper SPE146876 Presented at the SPE Reservoir Characterisation and Simulation Conference and Exhibition, Abu Dhabi, UAE, 9-11 October, 2011.

Cipolla, C.L., Lolon, E.P., Erdle, J.C., et al. Reservoir modeling in shale-gas reservoirs. SPE Reserv. Eval. Eng. 2010, 13(4): 638-653.

Clarkson, C.R. Production data analysis of unconventional gas wells: Review of theory and best practices. Int. J. Coal. Geol. 2013, 109: 101-146.

Fan, T., Zhang, G. Laboratory investigation of hydraulic fracture networks in formations with continuous orthogonal fractures. Energy 2014, 74: 164-173.

Guo, T., Zhang, S., Ge, H., et al. A new method for evaluation of fracture network formation capacity of rock. Fuel 2015, 140: 778-787.

Howarth, R.W., Ingraffea, A., Engelder, T. Natural gas: Should fracking stop? Nature 2011, 477(7364): 271.

Hughes, J.D. Energy: A reality check on the shale revolution. Nature 2013, 494(7437): 307.

Jiang, R., Xu, J., Sun, Z., et al. Rate transient analysis for multistage fractured horizontal well in tight oil reservoirs considering stimulated reservoir volume. Math Probl. Eng. 2014.

Jia, Y., Fan, X., Nie, R., et al. Flow modeling of well test analysis for porousvuggy carbonate reservoirs. Transport Porous Med. 2013, 97(2): 253-279.

King, G.E. Thirty years of gas shale fracturing: What have we learned? Paper SPE133456 Presented at the SPE Annual Technical Conference and Exhibition, Florence, Italy, 19-22 September, 2010.

Luo, W., Tang, C. Pressure-transient analysis of multiwing fractures connected to a vertical wellbore. SPE J. 2015, 20(2): 360-367.

Mayerhofer, M.J., Lolon, E.P., Warpinski, N.R., et al. What is stimulated reservoir volume? SPE Prod. Oper. 2010, 25(01): 89-98.

Mayerhofer, M.J., Lolon, E.P., Youngblood, J.E., et al. Integration of microseismic-fracture-mapping results with numerical fracture network production modeling in the Barnett Shale. Paper SPE102103 Presented at the SPE annual technical conference and exhibition, San Antonio, Texas, USA, 24-27 September, 2006.

Mănescu, C.B., Nuo, G. Quantitative effects of the shale oil revolution. Energy Policy 2015, 86: 855-866.

Meyer, B.R., Bazan, L.W. A discrete fracture network model for hydraulically induced fractures-theory, parametric and case studies. Paper SPE140514 Presented at the SPE hydraulic fracturing technology conference, The Woodlands, Texas, USA, 24-26 January, 2011.

Ozkan, E., Brown, M.L., Raghavan, R.S., et al. Comparison of fractured horizontal-well performance in conventional and unconventional reservoirs. Paper SPE121290 Presented at the SPE western regional meeting, San Jose, California, 24-26 March, 2009.

Ozkan, E., Brown, M.L., Raghavan, R.S., et al. Comparison of fractured-horizontal-well performance in tight sand and shale reservoirs. SPE Reserv. Eval. Eng. 2011, 14(2): 248-259.

Patzek, T.W., Male, F., Marder, M. Gas production in the Barnett Shale obeys a simple scaling theory. P. Natl. Acad. Sci. USA 2013, 110(49): 19731-19736.

Rahman, M.M., Aghighi, M.A., Shaik, A.R. Numerical modeling of fully coupled hydraulic fracture propagation in naturally fractured poro-elastic reservoir. Paper SPE121290 Presented at the EUROPEC/EAGE Conference and Exhibition, Amsterdam, The Netherlands, 8-11 June, 2009.

Sang, Y., Chen, H., Yang, S., et al. A new mathematical model considering adsorption and desorption process for productivity prediction of volume fractured horizontal wells in shale gas reservoirs. J. Nat. Gas Sci. Eng. 2014, 19: 228-236.

Stalgorova, E., Louis, M. Practical Analytical Model To Simulate Production of Horizontal Wells With Branch Fractures. Paper SPE162515 Presented at the SPE Canadian Unconventional Resources Conference, Calgary, Alberta, Canada, 30 October-1 November, 2012.

Stalgorova, E., Mattar, L. Analytical model for history matching and forecasting production in multifrac composite systems. Paper SPE162516 Presented at the SPE Canadian Unconventional Resources Conference, Calgary, Alberta, Canada, 30 October-1 November, 2012.

Stalgorova, K., Mattar, L. Analytical model for unconventional multifractured composite systems. SPE Reserv. Eval. Eng. 2013, 16(3): 246-256.

Stehfest, H. Algorithm 368: Numerical inversion of Laplace transforms [D5]. Commun. Acm. 1970, 13(1): 47-49.

Suliman, B., Meek, R., Hull, R., et al. Variable stimulated reservoir volume (SRV) simulation: eagle ford shale case study. Unconventional Resources Technology Conference, Denver, Colorado, 12-14 August, 2013.

Tian, L., Xiao, C., Liu, M., et al. Well testing model for multi-fractured horizontal well for shale gas reservoirs with consideration of dual diffusion in matrix. J. Nat. Gas Sci. Eng. 2014, 21: 283-295.

Van, Everdingen, A.F., Hurst, W. The application of the Laplace transformation to flow problem in reservoirs. Journal of Petroleum Technology 1949, 1(12): 305-324.

Wang, H., Liao, X., Zhao, X. Study of tight oil reservoir flow regimes in different treated horizontal well. J. Energy. Inst. 2015, 88(2): 198-204.

Wang, Q., Chen, X., Jha, A.N., et al. Natural gas from shale formationthe evolution, evidences and challenges of shale gas revolution in United States. Renew. Sust. Energ. Rev. 2014, 30: 1-28.

Weng, X., Kresse, O., Chuprakov, D., et al. Applying complex fracture model and integrated workflow in unconventional reservoirs. J. Petrol Sci. Eng. 2014, 124: 468-483.

Wu, K. Numerical modeling of complex hydraulic fracture development in unconventional reservoirs. The University of Texas at Austin, USA, 2014.

Xu, J., Guo, C., Teng, W., et al. Production performance analysis of tight oil/gas reservoirs considering stimulated reservoir volume using elliptical flow. J. Nat. Gas Sci. Eng. 2015, 26: 827-839.

Yu, W., Zhang, T., Du, S., et al. Numerical study of the effect of uneven proppant distribution between multiple fractures on shale gas well performance. Fuel 2015, 142: 189-198.

Zerzar, A., Bettam, Y. Interpretation of multiple hydraulically fractured horizontal wells in closed systems. Paper SPE162516 Presented at the Canadian International Petroleum Conference, Calgary, Alberta, 8-10 June, 2004.

Zhao, Y., Zhang, L., Luo, J., et al. Performance of fractured horizontal well with stimulated reservoir volume in unconventional gas reservoir. J. Hydrol. 2014, 512: 447-456.

Appendix A

Dimensionless variables:

$$p_D = \frac{2\pi k_{f_1} h(p_i - p_1)}{q_{sc}\mu},\ t_D = \frac{k_{f1}t}{(\phi_1 C_{t1})_{m+f}\mu L^2},\ z_{1D} = \frac{z}{L},$$

$$r_D = \frac{r}{L},\ h_D = \frac{h}{L},\ M = \left(\frac{k_{f1}}{\mu}\right) / \left(\frac{k_{f2}}{\mu}\right),$$

$$\eta = \left(\frac{k_{f1}}{(\phi_1 \mu C_{t1})_{m+f}}\right) / \left(\frac{k_{f2}}{(\phi_2 \mu C_{t2})_{m+f}}\right),\ \lambda_1 = \frac{k_{m1}L^2}{k_{f1}{R_1}^2},$$

$$\lambda_2 = \frac{k_{m2}L^2}{k_{f2}{R_2}^2},\ \omega_1 = \frac{\phi_{f1}C_{tf1}}{\phi_{f1}C_{tf1} + \phi_{m1}C_{tm1}},$$

$$\omega_2 = \frac{\phi_{f2}C_{tf2}}{\phi_{f2}C_{tf2} + \phi_{m2}C_{tm2}},\ r_{m1D} = \frac{r}{R_1},\ r_{m2D} = \frac{r}{R_2}$$

Appendix B

Inner region

Using the dimensionless variables (see Appendix A) for Eq. 1 - 4, the following equations can be derived:

$$\frac{1}{{r^2}_{m1D}} \frac{\partial}{\partial r_{m1D}} \left({r^2}_{m1D} \frac{\partial p_{m1D}}{\partial r_{m1D}} \right) = \frac{(1-\omega_1)}{\lambda_1} \frac{\partial p_{m1D}}{\partial t_D} \quad (0 \le r_{m1D} \le 1) \tag{B1}$$

$$p_{m1D}\left(r_{m1D}, 0\right) = 0 \tag{B2}$$

$$\left.\frac{\partial p_{m1D}}{\partial r_{m1D}}\right|_{r_{m1D}=0} = 0 \tag{B3}$$

$$\left. p_{m1D}\right|_{r_{m1D}=1} = p_{f1D} \tag{B4}$$

Taking Laplace transformation to t_D, Eq. B1 - Eq. B4 becomes:

$$\frac{1}{{r^2}_{m1D}} \frac{\partial}{\partial r_{m1D}} \left({r^2}_{m1D} \frac{\partial \overline{p}_{m1D}}{\partial r_{m1D}} \right) = \frac{(1-\omega_1)}{\lambda_1} u\overline{p}_{m1D} \quad (0 \le r_{m1D} \le 1) \tag{B5}$$

$$\overline{p}_{m1D}\left(r_{m1D}, 0\right) = 0 \tag{B6}$$

$$\left.\frac{\partial \overline{p}_{m1D}}{\partial r_{m1D}}\right|_{r_{m1D}=0} = 0 \tag{B7}$$

$$\left. \overline{p}_{m1D}\right|_{r_{m1D}=1} = \overline{p}_{f1D} \tag{B8}$$

Solve the equations Eq. B5 - Eq. B8:

$$\overline{p}_{m1D}\left(r_{mD}, u\right) = \frac{\overline{p}_{f1D}}{\sinh\left(\sqrt{\frac{(1-\omega_1)u}{\lambda_1}}\right)} \frac{\sinh\left(r_{m1D}\sqrt{\frac{(1-\omega_1)u}{\lambda_1}}\right)}{r_{m1D}} \tag{B9}$$

Using the dimensionless variables (see Appendix A), Eq. 5 can be derived:

$$\frac{1}{r_D}\frac{\partial}{\partial r_D}\left(r_D\frac{\partial p_{f1D}}{\partial r_D}\right)=\omega_1\frac{\partial p_{f1D}}{\partial t_D}+3\lambda_1\frac{\partial p_{m1}}{\partial r_{m1D}}\Big|_{r_{mD}=1} \tag{B10}$$
$$(0\le r_D\le r_{1D})$$

Taking Laplace transformation to t_D, Eq. B10 becomes:

$$\frac{1}{r_D}\frac{\partial}{\partial r_D}\left(r_D\frac{\partial \overline{p}_{f1D}}{\partial r_D}\right)=\omega_1 u\overline{p}_{f1D}+3\lambda_1\frac{\partial \overline{p}_{m1}}{\partial r_{m1D}}\Big|_{r_{mD}=1} \tag{B11}$$
$$(0\le r_D\le r_{1D})$$

With Eq. B9 and Eq. B11, the flow equation in inner region can be derived:

$$\frac{1}{r_D}\frac{\partial}{\partial r}\left(r_D\frac{\partial \overline{p}_{f1D}}{\partial r_D}\right)=f_1\overline{p}_{f1D}$$
$$(0\le r_D\le r_{1D})$$
$$f_1=\omega_1 u+3\lambda_1\left(\sqrt{\frac{(1-\omega_1)}{\lambda_1}u}\coth\left(\sqrt{\frac{(1-\omega_1)}{\lambda_1}u}\right)-1\right) \tag{B12}$$

Outer region

Using the dimensionless variables (see Appendix A) for the above equations, the following equations can be derived:

$$\frac{1}{r^2{}_{m2D}}\frac{\partial}{\partial r_{m2D}}\left(r^2{}_{m2D}\frac{\partial p_{m2D}}{\partial r_{m2D}}\right)=\frac{(1-\omega_2)}{\lambda_2}\eta\frac{\partial p_{m2D}}{\partial t_D} \tag{B13}$$
$$(0\le r_{m2D}\le 1)$$

$$p_{m2D}\left(r_{m2D},0\right)=0 \tag{B14}$$

$$\frac{\partial p_{m2D}}{\partial r_{m2D}}\Big|_{r_{m2D}=0}=0 \tag{B15}$$

$$p_{m2D}\Big|_{r_{m2D}=1}=p_{f2D} \tag{B16}$$

Taking Laplace transformation to t_D, Eq. B13 - Eq. B16 becomes:

$$\frac{1}{r^2{}_{m2D}}\frac{\partial}{\partial r_{m2D}}\left(r^2{}_{m2D}\frac{\partial \overline{p}_{m2D}}{\partial r_{m2D}}\right)=\frac{(1-\omega_2)}{\lambda_2}u\overline{p}_{m2D} \tag{B17}$$
$$(0\le r_{m2D}\le 1)$$

$$\overline{p}_{m2D}\left(r_{m2D},0\right)=0 \tag{B18}$$

$$\frac{\partial \overline{p}_{m2D}}{\partial r_{m2D}}\Big|_{r_{m2D}=0}=0 \tag{B19}$$

$$\overline{p}_{m2D}\Big|_{r_{m2D}=1}=\overline{p}_{f2D} \tag{B20}$$

Solve the equations Eq. B17 - Eq. B20:

$$\overline{p}_{m2D}\left(r_{m2D},u\right)=\frac{\overline{p}_{f2D}}{\sinh\left(\sqrt{\frac{(1-\omega_2)}{\lambda_2}u\eta}\right)}\frac{\sinh\left(r_{m2D}\sqrt{\frac{(1-\omega_2)}{\lambda_2}u\eta}\right)}{r_{m2D}} \tag{B21}$$

Using the dimensionless variables, the following equation can be derived:

$$\frac{1}{r_D}\frac{\partial}{\partial r}\left(r_D\frac{\partial p_{f2D}}{\partial r_D}\right)=\omega_2\eta\frac{\partial p_{f2D}}{\partial t_D}+3\lambda_2\frac{\partial p_{m2}}{\partial r_{mD}}\Big|_{r_{mD}=1} \quad (r_{1D}\le r_D\le\infty_1) \tag{B22}$$

Taking Laplace transformation to t_D, Eq. B17 - Eq. B20 becomes:

$$\frac{1}{r_D}\frac{\partial}{\partial r}\left(r_D\frac{\partial \overline{p}_{f2D}}{\partial r_D}\right)=\omega_2\eta u\overline{p}_{f2D}+3\lambda_2\frac{\partial \overline{p}_{m2}}{\partial r_{m2D}}\Big|_{r_{m2D}=1} \quad (r_{1D}\le r_D\le\infty) \tag{B23}$$

With Eq. B21 and Eq. B23, the flow equation in inner region can be derived:

$$\frac{1}{r_D}\frac{\partial}{\partial r}\left(r_D\frac{\partial \overline{p}_{f2D}}{\partial r_D}\right)=f_2\overline{p}_{f2D} \quad (r_{1D}\le r_D\le\infty)$$

$$f_2=\omega_2 u\eta+3\lambda_2\left(\sqrt{\frac{(1-\omega_2)}{\lambda_2}u\eta}\coth\left(\sqrt{\frac{(1-\omega_2)}{\lambda_2}u\eta}\right)-1\right) \quad (r_{1D}\le r_D\le\infty) \tag{B24}$$

Appendix C

To consider the finite conductivity fracture in transient pressure or rate analysis, the method proposed by Luo et al. (2014) was used.

Flow in hydraulic fracture can be described as:

$$\frac{\partial}{\partial Fx}\left(k_{Fl}\frac{\partial p_{Fl}}{\partial Fx}\right)+\frac{\partial}{\partial Fy}\left(k_{Fl}\frac{\partial p_{Fl}}{\partial Fy}\right)=0 \quad 0<Fx<Fx_{max} \tag{C1}$$

For the second term of Eq. C1, we can deal with it as follows:

$$\frac{\partial}{\partial Fy}\left(k_{Fl}\frac{\partial p_{Fl}}{\partial Fy}\right)=\frac{2}{W_{Fl}}\left(k_{Fl}\frac{\partial p_{Fl}}{\partial Fy}\Big|_{Fy=Fy_o+\frac{W_{Fl}}{2}}-k_{Fl}\frac{\partial p_{Fl}}{\partial Fy}\Big|_{Fy=Fy_o}\right) \tag{C2}$$

Combining Eq. C1 and Eq. C2 yields:

$$\frac{\partial}{\partial Fx}\left(k_{Fl}\frac{\partial p_{Fl}}{\partial Fx}\right)+\frac{2}{W_{Fl}}\left(k_{Fl}\frac{\partial p_{Fl}}{\partial Fy}\Big|_{Fy=Fy_o+\frac{W_{Fl}}{2}}-k_{Fl}\frac{\partial p_{Fl}}{\partial Fy}\Big|_{Fy=Fy_o}\right)=0 \tag{C3}$$

There is no flux in y direction, so Eq. C3 becomes:

$$\frac{\partial}{\partial Fx}\left(k_{Fl}\frac{\partial p_{Fl}}{\partial Fx}\right)+\frac{2}{W_{Fl}}k_{Fl}\frac{\partial p_{Fl}}{\partial Fy}\Big|_{Fy=Fy_o+\frac{W_{Fl}}{2}}=0 \tag{C4}$$

At the interface of natural fracture and hydraulic fracture:

$$\frac{k_{Fl}}{\mu}\frac{\partial p_{Fl}}{\partial Fy}\Big|_{Fy=F_{yo}+\frac{W_{Fl}}{2}}=\frac{k_{f1}}{\mu}\frac{\partial p_{f1}}{\partial Fy}\Big|_{Fy=F_{yo}+\frac{W_{Fl}}{2}} \tag{C5}$$

Combining Eq. C4 and Eq. C5 yields:

$$\frac{\partial}{\partial Fx}\left(k_{Fl}\frac{\partial p_{Fl}}{\partial Fx}\right)+\frac{2}{W_{Fl}}k_{f1}\frac{\partial p_{Fl}}{\partial Fy}\Big|_{Fy=Fy_o+\frac{W_{Fl}}{2}}=0 \tag{C6}$$

Assume the production of the fracture is q_{Fl}, we get:

$$\frac{k_{Fl}}{\mu}\frac{\partial p_{Fl}}{\partial Fx}\Big|_{Fx=0}\cdot\frac{W_{Fl}h}{2}=\frac{q_{Fl}}{2} \tag{C7}$$

Close boundary for fracture:

$$\frac{k_{Fl}}{\mu}\frac{\partial p_{Fl}}{\partial Fx}\Big|_{Fx=Fx_{max}}=0 \tag{C8}$$

The relationship between the natural fracture flux and hydraulic fracture line source is:

$$q_L=2h\frac{k_{f1}}{\mu}\frac{\partial p_{f1}}{\partial Fy}\Big|_{Fy=Fyo+\frac{W_{Fl}}{2}} \tag{C9}$$

Using the dimensionless variables, and Laplace transformation, Eq. C6 - Eq. C9 becomes:

$$\frac{\partial^2\overline{p}_{FlD}}{\partial Fx_D^2}+\frac{2}{R_{FlD}}\frac{\partial\overline{p}_{flD}}{\partial Fy_D}\Big|_{Fy_D=Fy_{OD}+\frac{W_{FlD}}{2}}=0 \tag{C10}$$

$$\frac{\partial\overline{p}_{FlD}}{\partial Fx_D}\Big|_{x_D=0}=-\frac{2\pi}{R_{FlD}}\overline{q}_{FlD} \tag{C11}$$

$$\frac{\partial\overline{p}_{FD}}{\partial Fx_D}\Big|_{x_D=L_{FlD}}=0 \tag{C12}$$

$$q_{LD}=-\frac{1}{\pi}\frac{\partial p_{f1D}}{\partial Fy_D}\Big|_{Fy_D=Fy_{OD}+\frac{W_{FlD}}{2}} \tag{C13}$$

Where:

$$R_{FlD}=\frac{k_{Fl}W_{Fl}}{k_mL_{ref}},W_{FlD}=\frac{W_{Fl}}{L_{ref}},q_{FlD}=\frac{q_{Fl}}{Q},q_{LD}=\frac{L_{ref}q_L}{Q} \tag{C14}$$

We can get:

$$\overline{p}_{wD}-\overline{p}_{FlD}=\frac{2\pi}{R_{FlD}}\left[x_D\overline{q}_{FlD}-\int_0^{x_D}\int_0^{v}\bar{\tilde{q}}_{LD}dx_Ddv\right] \tag{C15}$$

Discrete the Eq. C15:

$$\overline{p}_{wD}-\overline{p}_{FljD}\left(Fxj\right)=\frac{2\pi}{R_{FlD}}\left[Fx_{jD}\sum_{k=1}^{n}\overline{q}_{LkD}\Delta Fx_D-\sum_{i=1}^{j-1}\overline{q}_{LjD}\left(j-i\right)\Delta Fx_D^2-\overline{q}_{LiD}\frac{\Delta Fx_D^2}{8}\right] \tag{C16}$$